
INFLUENCE OF Cu²⁺-DOPED FeMgO NANOMATERIALS ON THE DEHYDROGENATION AND DEHYDRATION OF ETHANOL

Sahar A. El-Molla^{1*}, Ahmed A. Farghali², Hala R. Mahmoud¹, Ahmed M. Abdullah³

¹Department of Chemistry, Faculty of Education, Ain Shams University, Roxy 11757, Cairo, Egypt

²Department of Materials Science and Nanotechnology, Faculty of Postgraduate Studies for Advanced Sciences, Beni-Suef University, Egypt

³Department of Optics, High Institute of Optics Technology (HIOT), Cairo, Egypt

*Corresponding author: email saharelmolla@yahoo.com, Fax: +202 22581243.

ABSTRACT

Nanoparticles of iron oxide supported on MgO were prepared by wet impregnation method with loadings varied over 0.02– 0.25 mol Fe₂O₃ to 0.1 mol MgO. The effects of Cu²⁺ doping on the surface and catalytic properties of Fe₂O₃/MgO system have been investigated. The extent of Iron oxide loading was fixed at 10 mol % and the CuO dopant concentration was varied between 1 and 7mol%. Pure and the treated samples were subjected to heat treatment at 500°C. The prepared catalysts were characterized by XRD, HRTEM, S_{BET}-measurements and catalytic conversion of ethanol by flow method to yield ethylene and acetaldehyde. The particles of all samples have a uniform cube like with irregular shapes. Increasing the Fe₂O₃ content to 10 mol % led to increasing the catalytic activity and selectivity to ethylene formation, however, the activity decreases above this limit. Cu²⁺ doping increases the catalytic activity of Fe₂O₃/MgO catalyst towards the dehydrogenation of ethanol and all CuFeMgO samples are selective to acetaldehyde with 100%.

Keywords: Fe₂O₃/MgO catalyst, Cu²⁺ doping, Dehydrogenation selectivity, Nanomaterials.

1. INTRODUCTION

Fe₂O₃-based nanomaterials are of significant importance in catalytic processes, especially in oxidation ones [1]. α-Fe₂O₃ is used for many applications because of its non-toxicity, low processing cost, availability, and high resistance to oxidative change [2,3]. Its disadvantages can be combined by the low thermal stability against sintering and crystal growth which are typically accompanied by considerable surface area reduction and hence, rapid deactivation in catalytic investigations [3]. Therefore, modification of Iron oxide by mixing it with other oxides attracted the attention of many researchers [2,3]. Mixed oxide catalysts usually exhibit modified textural, structural, and catalytic properties as compared with their corresponding metal oxides [4]. Supported metal oxides [5] usually exhibit modification in its textural, structural, and catalytic properties [4]. It is known that the activity and selectivity of a large variety of catalysts can be modified by loading on a finely

divided support and doping with certain foreign oxides [6]. Doping system containing transition metal oxides with certain foreign oxides is accompanied by significant modifications in their thermal stability, electrical, optical, magnetic, surface, and catalytic properties [7]. Doping the Fe-Cr composition with CuO resulted in an evident enhancement in catalyst activity of the water-gas shift (WGS) reaction [8]. Doping the ceramics with 1 mol% CuO exhibited enhanced electrical properties [9]. Doping NiO with CuO caused a significant increase in the catalytic activity towards H₂O₂ decomposition [10]. This present paper describes the effects of Fe₂O₃ loading, CuO doping as well as calcination temperature on the Fe₂O₃ /MgO nanomaterials for the catalytic conversion of ethanol. The as-prepared nanomaterials were characterized by X-ray diffraction (XRD), high-resolution transmission electron microscope (HR-TEM) and N₂ adsorption–desorption isotherms and the catalytic conversion of ethyl alcohol at 150–350 °C using the flow method.

2. EXPERIMENTAL

2.1. Materials

Magnesium carbonate (MgCO_3 , Adwic), Magnesium nitrate, ($\text{Mg}(\text{NO}_3)_2 \cdot 6\text{H}_2\text{O}$, BDH), Iron nitrate ($\text{Fe}(\text{NO}_3)_3 \cdot 9\text{H}_2\text{O}$, Loba), Copper nitrate ($\text{Cu}(\text{NO}_3)_2 \cdot 3\text{H}_2\text{O}$, Loba), oxalic acid dihydrate, ($\text{C}_2\text{H}_2\text{O}_4 \cdot 2\text{H}_2\text{O}$, Adwic), urea, $[(\text{NH}_2)_2\text{CO}]$, Adwic], absolute ethanol, $\text{C}_2\text{H}_5\text{OH}$ (Adwic, 99.9 % purity) and Ammonia solution, (NH_4OH , Alpha). Bi-distilled water was used to prepare all the solutions.

2.2. Preparation of $\text{Fe}_2\text{O}_3/\text{MgO}$ nanomaterials

2.2.1. Impregnation method

The catalysts $\text{Fe}_2\text{O}_3/\text{MgO}$ with (0 – 100) mol % were prepared by the impregnation method. The procedure was as follows: the required quantity of $\text{Fe}(\text{NO}_3)_3 \cdot 9\text{H}_2\text{O}$ was dissolved in a minimum amount of bi-distilled water and this solution was added to the MgCO_3 support to make a paste. The prepared catalysts were dried in an air oven at $110\text{ }^\circ\text{C}$ for 8 h and finally calcined at $500\text{ }^\circ\text{C}$ for 3 h. The formula $x\text{FeMgO}$ will be used throughout the paper to represent the different composites where x refers to the Fe^{3+} loading.

2.3. Preparation of CuO doped $\text{Fe}_2\text{O}_3/\text{MgO}$ nanomaterials

The CuO-doped $0.10\text{Fe}_2\text{O}_3/\text{MgO}$ nanomaterials were prepared using a known mass of MgCO_3 impregnated with solutions containing a constant amount of iron nitrate and different proportions of copper nitrate. The pastes obtained were dried at $110\text{ }^\circ\text{C}$ then calcined in air at $500\text{ }^\circ\text{C}$ for 3 h. The molar ratios of CuO in the composition were set for 1, 3, 5 and 7%. The formula of the prepared catalysts was nominated as $y\text{CuFeMgO}$ where y refers to the CuO loading.

2.4. Catalyst characterization

Powder prepared catalyst was characterized and studied by X-ray diffraction (XRD) study which carried out using Bruker Axs D8 Advance X-ray diffractometer (Germany). $\text{CuK}\alpha 1$ irradiation ($\lambda = 0.15404\text{ \AA}$) was used

with a scan rate of $2\theta/\text{min}$. Specific surface areas of the different catalysts were determined by N_2 adsorption–desorption measurements at $-196\text{ }^\circ\text{C}$ by employing the Brunauer–Emmet–Teller (BET) method (Quantachrome NOVA 2000 Autosorb Gas Sorption System) (USA), and the pore size of the samples was calculated from desorption branch of the isotherm by the Barrett, Joyner and Halenda (BJH) method. Prior to N_2 adsorption, the sample was outgassed at $200\text{ }^\circ\text{C}$ for 2 h to desorb moisture adsorbed on the surface and inside the pores. The morphology of the catalysts was observed by high-resolution transmission electron microscope (HR-TEM) microanalysis system (JEM-2100CX (JEOL)).

2.5. Catalytic activity test

The catalytic oxidation of ethanol was performed in a fixed-bed flow reactor at atmospheric pressure. Typically, 100 mg of sample was placed in a Pyrex glass reactor tube (10 mm i.d.). Argon gas was used as a carrier and the ethanol vapor was introduced into the reactor through an evaporator/saturator at the ethanol pressure equal 100 Torr with a flow rate of 30 ml/min. Before every run the catalyst sample was activated by heating at $300\text{ }^\circ\text{C}$ in a current of argon for 1h then cooled to the reaction temperature. The steady-state tests were conducted isothermally every $25\text{ }^\circ\text{C}$ from $100\text{ }^\circ\text{C}$ to $400\text{ }^\circ\text{C}$ and the gas products were analyzed by a flame ionization detection (FID) of Perkin-Elmer Auto System XL Gas Chromatograph (GC) equipped with a packed column (10% squalane supported on chromosorb, 4m). The temperature of the detector was $250\text{ }^\circ\text{C}$ and the column temperature was programmed at $60\text{ }^\circ\text{C}$.

3. RESULTS AND DISCUSSION

3.1. X-ray diffraction analysis

X-ray diffractograms (XRD) of 0.02FeMgO , 0.1FeMgO and 0.25FeMgO catalysts calcined at $500\text{ }^\circ\text{C}$ are presented in Fig. 1a. The XRD of pure MgO and doped 0.1FeMgO samples with 0.4, 1.22, 2.05 and 2.91 wt% CuO followed by calcination at 500

°C are shown in Fig. 1b. It was clearly noticed that the XRD diffractogram of the FeMgO sample exhibits peaks due to MgO phase (periclase) (JCPDS 4-829) with a moderate degree of ordering. No characteristic peaks related to Fe₂O₃ or MgFe₂O₄ phases were detected by XRD in samples with small contents of Fe₂O₃. Increasing the extent of loading to 10 mol% results in a decrease in degree of ordering of MgO phase, suggesting a high dispersion and small size of the iron species in the FeMgO system [29]. So, magnesium oxide may act as a convenient support to hematite. Increasing the Fe₂O₃ content to 25 mol% resulted in a drastic decrease in the degree of ordering of all peaks related to MgO phase together with the appearance of peaks related to Fe₂O₃ and MgFe₂O₄ phases. A further observation revealed that 0.1 FeMgO and 0.25 FeMgO samples had broader diffraction peaks, indicating slightly poorer crystallinity and smaller sizes as shown by particle dimension calculation using the Scherrer equation [33]. The average crystallite sizes of MgO phase decrease with increasing the extent of loading Fe₂O₃ as shown in Table 1.

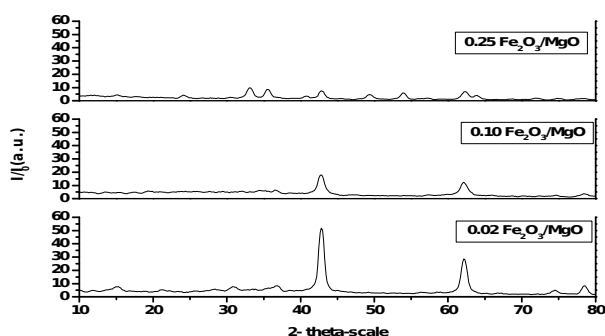


Fig. 1a. XRD of FeMgO solids with different extent of Fe₂O₃ loading calcined at 500 °C.

The role of CuO-doping on the structural characteristics of Fe₂O₃/MgO system followed by calcination at 500 °C was investigated (Fig. 1b). Inspection of Fig. 1b and Table 1 shows the followings: (i) all phases present in the different investigated solids are of nanosized range (3–78 nm). (ii) Doping with CuO resulted

in appearance of diffraction lines having very small relative intensities located at d spacing = 2.43Å (JCPDS 5-667) corresponding to Cu₂O phase. This line is common with MgO phase. Cu₂O show common diffraction lines at d = 2.43, 2.11, 1.48Å makes their distinction a difficult task. The line intensity % at d-spacing 2.43Å exceeds 10 % for MgO phase which support the possible formation of Cu₂O phase. (iii) Possible formation of CuFe₂O₄ phase which having common diffraction lines common with MgO phase resulted by CuO doping.

The absence of diffraction peaks due to Fe₂O₃ phase might indicate its presence in finely divided state beyond the detection limit of X-ray diffractometer. (iv) The degree of crystallinity of MgO phase decreased by the addition of small amount of CuO. A further increase in the amount of CuO above this limit brought about a progressive increase in the degree of ordering of this phase, then decreased again. In fact, the areas of the main peak of MgO phase measured 23.6, 24.5, 28.9, 26.1 and 29.6 a.u. for pure and samples doped with 0.4, 1.22, 2.05 and 2.91 wt% CuO, respectively. (v) Increasing the concentrations up to 2.91 wt% CuO exerted a limited effect on the crystallite size of MgO phase. Increasing the dopant concentration to 2.91 mol% resulted in a measurable increase in the crystallite size of MgO phase. (vi) The calculated value of lattice constant of MgO phase decreases by adding of Fe₂O₃ and increased by increasing the amount of added CuO. This finding suggests that CuO-doping led to a measurable expansion of the lattice constant of MgO lattice. This expansion could be discussed in terms of the difference in the ionic size of host cation lattice (Mg²⁺) and Cu²⁺ cations which measure 0.72 and 0.73 Å, respectively. So, the substitution of some of Mg²⁺, in MgO lattice, by a portion of Cu²⁺ should normally accompanied by an increase in the lattice constant of MgO phase, i.e. an expansion of its lattice.

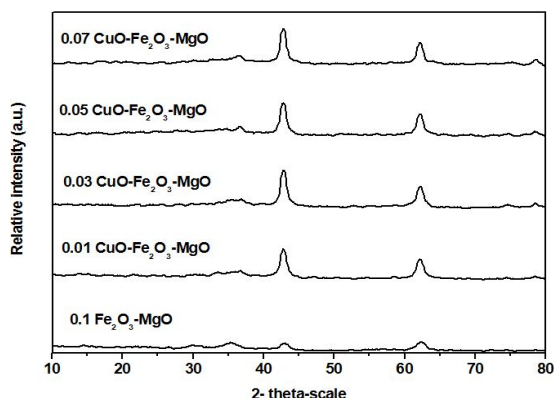


Fig. 1b. XRD of pure $\text{Fe}_2\text{O}_3/\text{MgO}$ solid and after doping with different amounts of CuO followed by calcination at 500°C .

Table 1. Structural characteristics of pure and CuO -doped solids calcined at 500°C .

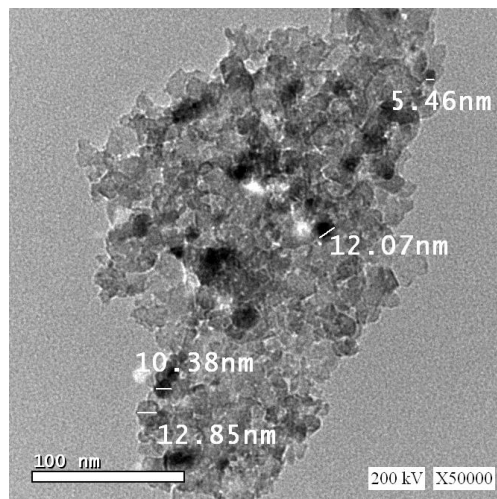
| $\text{Fe}_2\text{O}_3/\text{MgO}$ + $x\text{CuO}$ x (mole) | Relative intensity count (a.u.) | Crystallite size (nm) | α - Constant ^a (MgO) (Å) |
|---|--|--------------------------|--|
| | MgO | MgO | |
| 0.00 | 26.6 | 15.6 | 4.219 |
| 0.01 | 25.6 | 15.1 | 4.211 |
| 0.03 | 38.5 | 18.1 | 4.216 |
| 0.05 | 30.5 | 17.1 | 4.215 |
| 0.07 | 35.3 | 15.7 | 5.222 |

^a Standard value of lattice parameter (a -constant) of $\text{MgO} = 4.21\text{Å}$

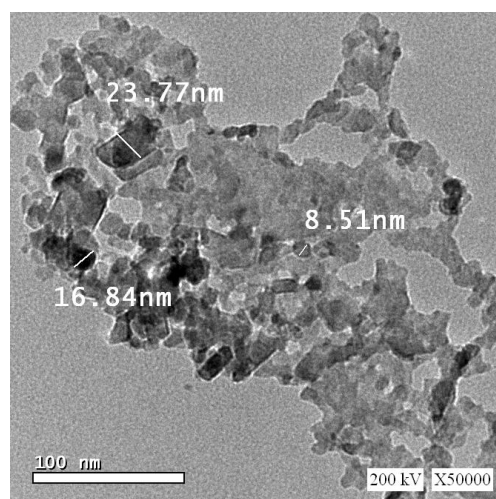
3.2. HR-TEM analysis

Fig.2 depicts the HR-TEM images of 0.1FeMgO and 0.03CuFeMgO nanomaterials calcined at 500°C . It can be seen from Fig. 2 that the particles of all catalysts have uniform spherical shapes. The TEM image of FeMgO solid contain aggregates of uniform trigonal shapes from MgO nanoparticles with an average diameter of 12 nm. (ii) TEM of CuFeMgO sample contains uniform spherical nanoparticles with an average diameter of 18nm. The average particle size of CuFeMgO calculated from the TEM micrographs is consistent with the average crystallite size obtained from the XRD measurement. Besides, there are very small darker spots highly dispersed in the oxide layer. These spots correspond to very small highly dispersed iron

oxide particles [14,15]. So, FeMgO and CuFeMgO samples calcined at 500°C contain randomly distributed and highly aggregated nanoparticles.



FeMgO



CuFeMgO

Fig.2.HR-TEM images of pure 0.1FeMgO and 0.03CuFeMgO nanomaterials calcined at 500°C .

3.3. Surface properties

The nitrogen adsorption isotherms of FeMgO and CuFeMgO were measured at 196°C . The isotherms obtained, not given here, are of type II of Brunauer's classification showing closed hysteresis loops. The specific surface areas were calculated from these adsorption isotherms by applying the BET equation [16].

The surface texture of FeMgO catalysts were previously investigated by two of authors[11] and the most important results were reported as followings: i) the addition of a small amount of Fe₂O₃ to the MgO support followed by calcination at 500°C resulted in an increase in S_{BET} of hematite. The increase in the Fe₂O₃ molar content to 10 mol% is accompanied by a limited decrease in S_{BET}. Increasing the Fe₂O₃ content to 25 mol% in this study was followed by an increase in surface area. Doping of FeMgO solids with CuO followed by calcination at 500°C led to a measurable decrease in its S_{BET}. The decrease in S_{BET} value of FeMgO sample due to CuO-doping can be explained in terms of possible formation of spinels were accompanied by a steady decrease in specific surface area, a consequence of consumption of CuO and possible formation of nano ferrite phases. (ii) presence of randomly distributed and highly aggregated nanoparticles as shown in HRTEM section.

According to the V_{L-t} plot curves, not given here, of the investigated samples, Fe₂O₃ has shown a mesoporous structure while the FeMgO one exhibits a microporous nanocomposite. Increasing Fe₂O₃ content produced sample consist of a mixture of meso- and micropores. The changes in the specific surface areas of the prepared and calcined samples can be explained as follows: i) the increase observed in the S_{BET} value of hematite due to loading on the MgO support can be discussed in the light of fine dispersion of the Fe₂O₃ particles on the surface of MgO [19]. The XRD peaks due to iron oxide were not detected in the investigated samples, indicating that the iron oxide phase exists in very small crystallite size i.e. nano size. The change from

mesoporous structure to microporous structure as a result of supporting iron oxide on magnesia is another factor. ii) The induced limited decrease in the surface area of FeMgO sample at 10 mol% due to the increase in the molar amount of Fe₂O₃ loading may be due to the creation of mesopores in addition to the micropores ;the presence of this mixture is accompanied by a decrease in surface area [11]. Another factor is the location of very small Fe₂O₃ crystallites in the magnesia pores [20]. While the observed increase in SBET-surface area in case of 0.25FeMgO sample may be due to formation porous ferrite compounds with crystal structure is different from other samples as shown in Fig. 1a in XRD section.

3.4. Catalytic conversion of ethanol over different investigated solids

3.4.1. Effect of extent of Fe₂O₃ loading on the activity Fe₂O₃/MgO system towards ethanol conversion

The catalytic conversion of ethanol was carried out over 0, 1, 2, 5, 10, 25 and 50 % Fe₂O₃ on MgO. The same catalytic reaction was also carried out over un-promoted MgO support. The detected products of ethanol conversion in presence of FeMgO were acetaldehyde, ethylene and diethyl ether (not shown).Figure (3) shows the effect of the extent of Fe₂O₃ loading in the Fe₂O₃ /MgO system on its catalytic activity expressed as the total conversion. Figures 4,5 show the selectivities toward ethylene and acetaldehyde formation at different reaction temperatures. It is noticed from figures (3-5) that: (i) MgO support exhibited relatively small catalytic activity, which increased by increasing the Fe₂O₃ content till 10% and then decreased. (ii) Supporting

Table 2 Some surface characteristics of some adsorbents

| Fe ₂ O ₃ /MgO + xCuO x (mole) | S _{BET} (m ² /g) |
|--|--------------------------------------|
| 0.00 | 45.36 |
| 0.03 | 35.55 |
| 0.07 | 34.20 |

| Fe ₂ O ₃ /MgO | S _{BET} (m ² /g) |
|-------------------------------------|--------------------------------------|
| 0.02 | 45.62 |
| 0.1 | 45.36 |
| 0.25 | 82.14 |

Fe₂O₃ on MgO material increased the catalytic activity and dehydration selectivity. (iii) the catalytic activity increased with increasing the reaction temperature from 200 to 400°C. (ii) All catalysts were highly selective to acetaldehyde 100% at 250°C; this selectivity decreases with increasing the reaction temperature. (iv) Small amounts of diethyl ether were detected. The obtained results can be explained as the followings: (i) the catalytic activity of FeMgO catalyst towards partial oxidation of ethanol to acetaldehyde depends on presence nano-iron oxide [21] supported on MgO. The observed increase in the catalytic activity of Fe₂O₃/MgO system due to increasing Fe₂O₃ content can be expressed as due to increase in the concentration of active sites involved in ethanol conversion (ii) The role of surface area is important in enhancing the high catalytic activity of FeMgO. This activity is due to consistency of the meso and micro structures

[11,15]. So, combination of smaller and larger mesopores could reduce transport limitations in catalysis, resulting in higher activities and better controlled selectivities [22]. It has been reported that Fe³⁺ has higher electronegativity as compared to Mg²⁺, and formation of solid solutions with medium-strength basic sites [23]. The observed decrease in the catalytic activity and selectivity of FeMgO with higher loadings i.e. > 10% Fe₂O₃ could be due to ferrite formation. (iv) Acetaldehyde is produced according to dehydrogenation mechanism involving nanosized Fe³⁺ ions and medium strength basic active sites [Mg(M)-O] with high density [24]. The observed high selectivity of the FeMgO catalyst for acetaldehyde production stresses the role of magnesium ferrite in partial oxidation to acetaldehyde, and supports the idea of disappearance of Fe₂O₃ phase. Fe₂O₃ is known as an active catalyst to total oxidation of methanol [25].

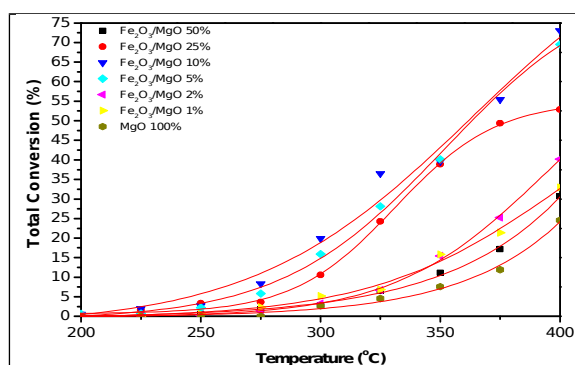


Fig. 3. Catalytic conversion of ethanol in presence of MgO and FeMgO samples with various Fe₂O₃ loadings.

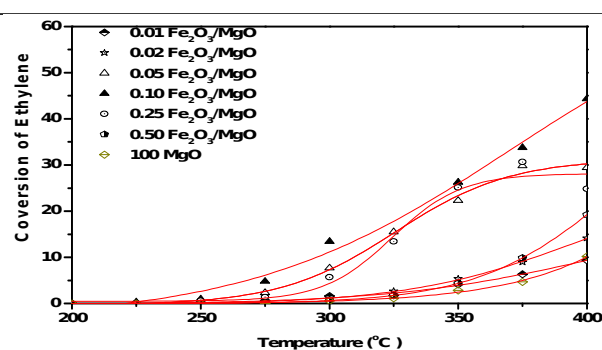


Fig.4. Conversion of ethanol to ethylene in presence of MgO and FeMgO samples with various Fe₂O₃ loadings.

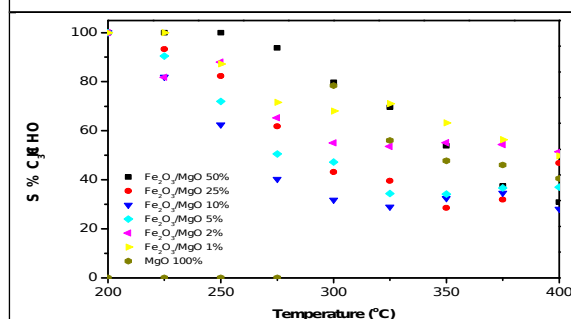


Fig.5. Selectivity to acetaldehyde in ethanol conversion over MgO and FeMgO samples Fe₂O₃ loadings.

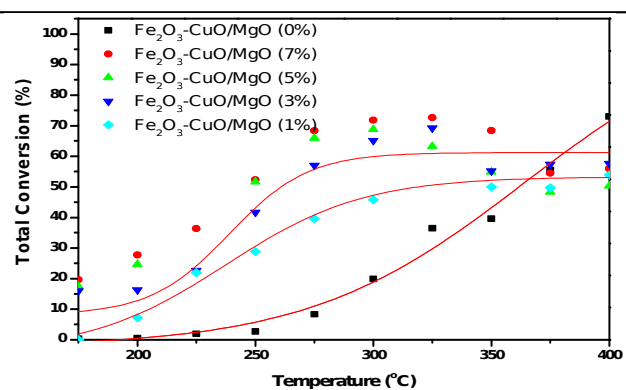


Fig. 6. Catalytic conversion of ethanol in presence of pure and CuO-doped FeMgO samples.

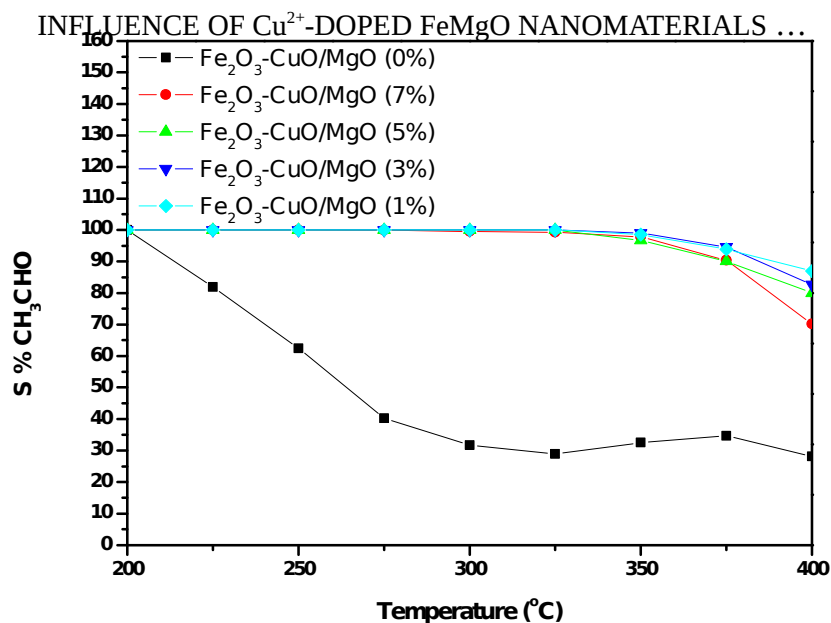


Fig.7. Selectivity to acetaldehyde in ethanol conversion over pure and CuO-doped FeMgO samples.

3.4.2. Effect of CuO doping on the activity and catalytic selectivity of $\text{Fe}_2\text{O}_3/\text{MgO}$

The catalytic conversion of ethanol was carried out over pure 0.1 $\text{Fe}_2\text{O}_3/\text{MgO}$ solids and that doped with increasing amounts of CuO followed by calcination at 500°C . Figures 6 and 7 show the effect of CuO doping on the total conversion of ethanol as a function of reaction temperature. It is noticed that: (i) increasing the amount of CuO to 0.07 mol resulted in an increase in the total conversion of ethanol. (ii) All the investigated solids acted as dehydrogenation catalysts and the selectivity towards acetaldehyde formation increases with increasing reaction temperature from 175 to 375°C and then decreases with increasing the reaction temperature. (iii) Increasing the CuO content from 0.01 to 0.07 mol increases selectivity to ethylene formation. It is clear from these results the role of CuO in increasing the selectivity towards dehydrogenation process with comparison to the un-doped sample.

It has been reported previously [26] that increasing the CuO content loaded on MgO resulted in formation of nano crystallites of CuO oxide. These finely divided particles may

be responsible for the high conversion for alcohols. Also, the presence of CuO with different oxidation states may play another role for increasing the alcohols conversion [27].

4. CONCLUSIONS

The objective of this paper is to study the effect of CuO doping onto $\text{Fe}_2\text{O}_3/\text{MgO}$ nanomaterials for the catalytic conversion of ethanol. The XRD and HR-TEM results showed that the CuO dopant had led to significantly increasing the crystallite size and lattice parameters of $\text{Fe}_2\text{O}_3/\text{MgO}$ nanomaterials. The catalytic activity of the binary oxides $\text{Fe}_2\text{O}_3/\text{MgO}$ nanomaterials was significantly increased by increasing the extent of loading of CuO till 10 wt%. The investigated samples were highly selective to dehydrogenation process. Besides, Fe_2O_3 loading increased the selectivity to the dehydration process to give ethylene. CuO doping, on the other hand, enhanced the stability to dehydrogenation even at high reaction temperatures.

REFERENCES

1. Wang H C, Chang S H, Hung P C, Hwang J F, Chang M B (2008) *Chemosphere* 71: 388-397.

2. Cao J-L, Wang Y, Yu X-L, Wang S-R, Wu S-H, Yuan Z-Y (2008). *Appl Catal B* 79: 26-34.
3. Liu XH, Shen K, Wang YG, Wang YQ, Guo YL, Guo ZL, Yong Z, Lu GZ (2008) *Catal Commun* 9: 2316–2318.
4. Wachs I.E (2005) *Catal Today* 100: 79-94.
5. Klabunde KJ, Khaleel A, Park D (1995) *HighTemp Mater Sci* 33: 99-105.
6. El-Molla SA (2006) *Appl Catal A* 298: 103–108.
7. El-Shobaky G A, Shouman M A, El-Khouly S M (2003) *Mater Lett* 58, 184–190.
8. Rhodes C., Hutchings G, J. (2003) *Phys. Chem* 5, 2719-2723.
9. Liu J., Zhu J., Li X., Wang, M, Zhu, X, Zhu J, Xiao D (2011) *Mater. Letters*, 65 ,948-950.
10. Turky AM (2003) *Appl Catal A* 247: 83–93.
11. El-Molla.S. A, Ali L. I. , Amin, N. H. , Ebrahim, A A, Mahmoud, H. R. (2012) *Chem. Papers* 66 (8) 722–732.
12. Tsoncheva T., Roggenbuck J. , Tiemann, M., Ivanova, L. , Paneva, D, Mitov, I. Minchev, C. (2008) *Micropor. Mesopor. Mater* 110, 339–346.
13. Cullity, B.D. (1967) *Elements of X-ray Diffraction*, 3rd ed., Addison-Wesley, Reading, MA.
14. K. Bachari, A. Touileb, A. Saadi, D. Halliche, O. Cherifi, (2010). *J. Porous Mater.* 17.
15. El-Molla. S.A, Mahmoud, H. R., (2013) *Mater. Research Bull.* 48 ,4105–4111.
16. Brunauer, S., Emmett, P. H., & Teller, E. (1938). *J. Amer. Chem. Soc.* 60, 309–319.
17. El-Molla, S.A., Hammed, M.N., El-Shobaky, G.A., (2004) *Mater. Lett.* 58 1003.
18. Mahmoud, H. R. Ph.D. of Teacher's Preparation in Science (2012).
19. Deraz, N. M. (2009). *Appl. Surface Sci.* 255, 3884–3890.
20. Radwan, N. R. E. (2006) *Appl. Catal. A* 299, 103–121.
21. Silva A.C., Oliveira D.Q.L., Oliveira, L.C.A., Anastácio, A.S., Ramalho T.C, Lopes J.H., Carvalho H.W.P., Torres C.E.R. (2009) *Appl. Catal. A*: 357, 79–84.
22. Meshkani, F. Rezaei, M. (2009) *Powder Technol.* 196, 85–88.
23. Ballarini, N., Cavani, F., Maselli, L., Montaletti, A., Passeri, S., Scagliarini, D., Flego C., Perego C. (2007) *J. Catal.* 251, 423–436.
24. Torres, G., Apesteguia, C.R., Di Cosimo, J.I., *Appl. Catal. A: Gen.* 317 (2007) 161–170.
25. Beale, A.M., Jacques, S.D.M., Sacaliuc-Parvalescu, E., O'Brien, M.G., Barnes, P, Weckhuysen, B.M. (2009) *Appl. Catal. A: Gen.* 363 ,143–152.
26. El-Molla, S. A., Ismail, S. A., Ibrahim, M. M., (2011). *J. Mex. Chem. Soc.* 55, 154.
27. El-Molla, S. A., El-Shobaky, G. A., Hammed, M. N., Amine, N. H., Sultan, S. N., (2013). *J. Mex. Chem. Soc.* 57, 1.